



Sub-acoustic resolution optical focusing through scattering using photoacoustic fluctuation guided wavefront shaping

MARCO A. INZUNZA-IBARRA,¹  EVOLENE PREMILLIEU,² CLEMENS GRÜNSTEIDL,^{1,3} RAFAEL PIESTUN,² AND TODD W. MURRAY^{1,*}

¹*Department of Mechanical Engineering, University of Colorado, Boulder, CO 80309, USA*

²*Department of Electrical, Computer, and Energy Engineering, University of Colorado, Boulder, CO 80309, USA*

³*Research Center for Non Destructive Testing, GmbH, 4040 Linz, Austria*

*todd.murray@colorado.edu

Abstract: Focusing light through turbid media using wavefront shaping generally requires a noninvasive guide star to provide feedback on the focusing process. Here we report a photoacoustic guide star mechanism suitable for wavefront shaping through a scattering wall that is based on the fluctuations in the photoacoustic signals generated in a micro-vessel filled with flowing absorbers. The standard deviation of photoacoustic signals generated from random distributions of particles is dependent on the illumination volume and increases nonlinearly as the illumination volume is decreased. We harness this effect to guide wavefront shaping using the standard deviation of the photoacoustic response as the feedback signal. We further demonstrate sub-acoustic resolution optical focusing through a diffuser with a genetic algorithm optimization routine.

© 2020 Optical Society of America under the terms of the [OSA Open Access Publishing Agreement](#)

1. Introduction

There has been a significant effort in recent years to develop high resolution optical techniques suitable for sensing and imaging inside of or through optically diffuse media. The applications in biomedical imaging are far-reaching and include optogenetics [1], photodynamic therapy [2], and early stage cancer detection [3]. The key technological hurdle that needs to be overcome is how to retain optical resolution when the optical field is diffused and access to ballistic photons is severely restricted. From a practical standpoint, this limits many state of the art optical imaging approaches that rely on ballistic photons, including optical coherence tomography and multi-photon microscopy, to superficial imaging in biological tissue at a depth of only a few hundred microns [4].

Optical wavefront shaping has emerged as a promising approach to control light propagation in scattering media [5,6]. Here, the idea is to harness scattered photons to enhance the resolution or signal-to-noise ratio of imaging systems operating in scattering environments. As the diffusive optical transport in scattering media is deterministic rather than random, it is possible to select an incident wavefront that compensates for scattering and leads to a well-developed optical focus through turbid media. The primary challenge lies in the selection of the input wavefront that will coerce the light to a target region to achieve the desired sensing or imaging goal. Various approaches for wavefront shaping have been demonstrated including phase conjugation [7], iterative optimization [8], and transmission matrix-based techniques [9].

In the majority of applications, wavefront shaping requires a sensing element, or guide star, that can provide information about the optical field at the target plane in a non-invasive manner. Wavefront shaping has been achieved using the second harmonic response from nanoparticles [10], fluorescent objects [11–14], and by modulating light using magnetic particles [15] or ultrasonically driven microbubbles [16]. All of these techniques require exogenous agents and

thus some access to the target plane. Kinetic guide stars have been demonstrated that use the modulated light induced by the intrinsic motion of the sample [17,18]. Alternative approaches based on the acousto-optic [19–24] and photoacoustic [25–29] response of a medium use a combination of ultrasound and light to guide light to a particular location. Acousto-optic guide stars use a focused ultrasound field to modulate the light within the light-sound interaction region. This is the fundamental basis for both the time reversed ultrasonically encoded technique as well as the time reversal of variance encoded focusing approach [19,24]. Photoacoustic guide stars, on the other hand, use ultrasound transducers to remotely detect photoacoustic signals generated by buried absorbers. The amplitude of the photoacoustic response is proportional to the optical fluence at the ultrasound transducer focus and can be used as feedback to guide the light to this location.

Photoacoustic guide stars are attractive for guiding light to absorbers within or behind scattering media using iterative wavefront shaping. The technique is non-invasive and the ultrasound transducer can guide the light to any absorber location within the sample volume. Optical wavefront shaping with photoacoustic feedback allows for an intensity enhancement within the ultrasound transducer focal region, but the optical spot-size that can be achieved is generally on the order of the diffraction limited ultrasound focal spot-size. Recent results indicate that it is possible to guide light to a focus smaller than the ultrasound spot-size by taking advantage of the spatial sensitivity of the ultrasonic transducer and using a genetic algorithm feedback routine to guide the light [26,28]. Nevertheless, this approach breaks down in the presence of noise when the optical speckle size is significantly smaller than the acoustic focus. Photoacoustic guided focusing of light has been shown to be more effective if the photoacoustic response of the sample is nonlinear. In a linear system, the transducer senses the integrated pressure within the focal zone and is less sensitive to how that pressure is distributed within that region. The integrated pressure is directly proportional to the integrated optical fluence. In a medium with a nonlinear response, the photoacoustic feedback signal continues to change as light is concentrated within the acoustic focus. In principle, a nonlinear feedback process can allow for light to be focused to a single optical speckle even if the speckle size is significantly smaller than the ultrasound focal spot. Lai et al. developed a dual pulse excitation approach to generate a nonlinear photoacoustic feedback signal based on the temperature dependence of the Grüneisen parameter [29]. Using this technique, they demonstrated optical focusing through a diffuser to a single speckle that was on the order of ten times smaller than the acoustic spot-size.

Here, we present an approach for focusing light through scattering media based on a nonlinear photoacoustic feedback signal elicited from a small vessel filled with flowing particles. The variance of the photoacoustic response, measured over multiple repetitions, is shown to be highly nonlinear with the optical spot-size, increasing dramatically as the optical spot-size is reduced well below the transducer focal spot-size. Sub-acoustic wavelength optical focusing through a diffuser is demonstrated using the standard deviation of the photoacoustic response as the feedback signal for a genetic algorithm optimization routine. Our technique is fundamentally different from previous kinetic guide-star mechanisms. In effect, it does not take advantage of the motion of individual particles but rather the randomness of particle distributions within the optical focal zone. Moreover, the nonlinear relationship between the optical spot-size and the photoacoustic variance is independent of the optical fluence. The ability to guide light to an optical focus significantly smaller than the acoustic focus represents an important step towards photoacoustic guided focusing to a single speckle within turbid media such as biological tissue, where the speckle size is on the order of half the wavelength.

2. Principle of the proposed method

We consider the photoacoustic response from a random distribution of particles inside of a cylindrical vessel as shown in Fig. 1(a). Upon pulsed laser illumination, each particle emits a

photoacoustic signal and the net photoacoustic response is the sum of the signals generated by each particle. At high particle concentrations, the photoacoustic signals from particles located in the interior of the tube tend to cancel while those emitted by particles at the boundary add coherently [30,31]. This is the origin of the limited-view problem in photoacoustic imaging where the interior of objects is hidden at high absorber concentrations while the coherent response from the object boundary is retained [32,33]. At lower concentrations, however, the signals from the interior of the tube no longer completely cancel, resulting in a photoacoustic response that appears random and depends on the locations of the individual particles. For flowing particles, the photoacoustic response will change for each different particle distribution and we quantify this variation by taking the standard deviation of the amplitude (σ_p) at each point in time over multiple measurements. The ratio of the standard deviation to the mean peak-to-peak amplitude (A_{pp}) of the photoacoustic response, referred to here as the normalized standard deviation (σ_N), increases as the particle concentration decreases [34]. We now consider what happens if we change the size of the optical beam incident on the flowing particles with a fixed concentration. If the optical beam is focused, then fewer particles are illuminated and there are fewer photoacoustic sources. This has a similar effect to reducing particle concentration, in that σ_N increases. Indeed, σ_N provides information on the size of the illumination volume and can be used to noninvasively probe optical beam size or as a guide star for wavefront shaping.

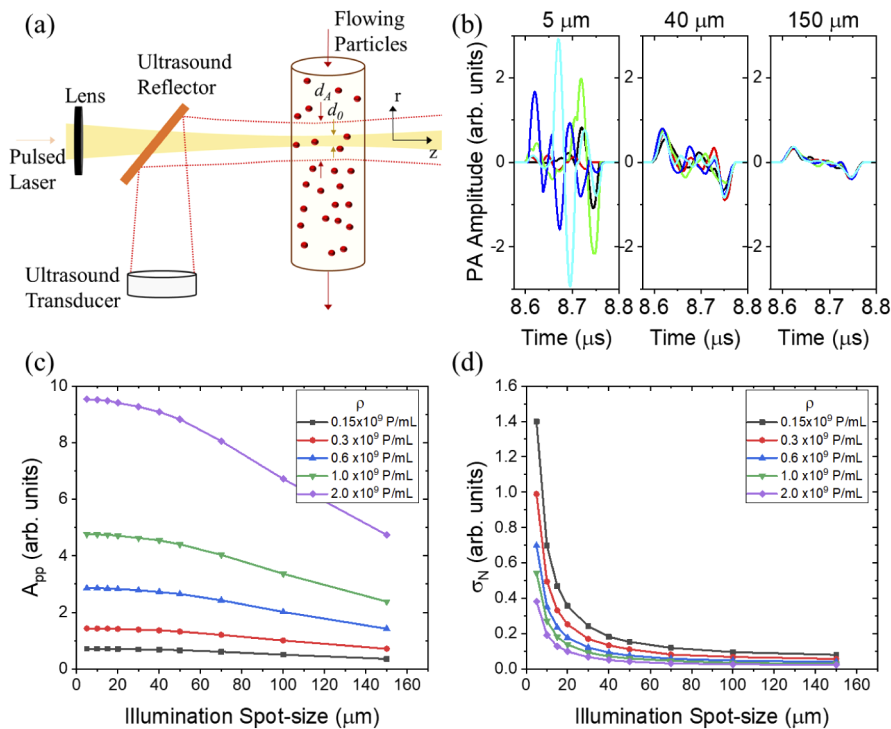


Fig. 1. Effect of spot-size on amplitude and variance of the photoacoustic response: (a) Geometry used for the numerical simulation. A pulsed laser illuminates flowing absorbers and a co-aligned ultrasonic transducer detects the particle photoacoustic emissions. (b) Five predicted photoacoustic single-shot responses from random absorbers of concentration $\rho = 0.3 \times 10^9$ particles/mL for different illumination spot-sizes. (c) A_{pp} as a function of illumination spot-size for several particle concentrations and (d) σ_N versus illumination spot-size for various particle concentrations.

We further elucidate this concept using a simulation. Here we consider particles randomly placed inside of a 200 μm diameter cylindrical tube illuminated with a Gaussian pulsed laser source with a full width at half maximum (FWHM) diameter of d_0 [see Fig. 1(a)]. The laser pulse is normalized such that the energy remains constant. Pulsed illumination of the particles leads to optical absorption, local heating, and emission of a pressure wave through the photoacoustic effect. The wave is detected by a transducer with a Gaussian focused spot-size of $d_A = 205 \mu\text{m}$ at FWHM and a focal length of 12.5 mm. We assume that the signal received by the focused transducer from each particle is a single cycle sine wave at 20 MHz, the central frequency of the transducer. We also assume that the particles are flowing fast enough to be in a random configuration at each laser shot. As the tube is small, we neglect beam spreading in the z direction within the tube and assume that both the acoustic and optical beams maintain a constant diameter through the tube interior. The amplitude of the signal received by the transducer from each particle is scaled by the particle position within the Gaussian excitation beam and the position within the Gaussian transducer focus. The net photoacoustic signal received by the transducer is the sum of the individual responses accounting for the propagation delay introduced between the absorber location and detection point.

The photoacoustic response for a particle concentration of $\rho = 0.3 \times 10^9$ particles/mL for three different optical excitation spot-sizes is shown in Fig. 1(b). In each plot, the photoacoustic signals for five different random distributions of particles are shown, and the time axis is zoomed in to view the photoacoustic arrival. For the 5 μm spot-size, the predicted responses show wide variability associated with the relatively small number of randomly distributed particles that are illuminated. As the spot-size is increased to 150 μm , the signals exhibit a uniform character and the coherent response from particles at the tube boundaries are evident. The simulation was run between 1,000 and 50,000 times to determine A_{pp} and σ_N for each spot-size, with a larger number of iterations used to achieve convergence of the mean for smaller spot-sizes. Note that the standard deviation of the amplitude at each time point is tracked, and σ_N is taken as the average value over a time window (8.68-8.72 μs) in the center of the arrival. In Fig. 1(c), we observe that A_{pp} does increase when the illumination spot decreases, an effect associated with the spatial sensitivity of the transducer across the focal zone [28], but this change becomes negligible as the optical spot gets small with respect to the acoustic focal spot. At a particle concentration of $\rho = 0.3 \times 10^9$ particles/mL, for example, A_{pp} increases by less than 3% when the spot-size is reduced from 30 μm to 5 μm . On the other hand, σ_N shows a dramatic increase with smaller spot-sizes as shown in Fig. 1(d). Taking the same particle concentration, σ_N increases by nearly 600% as the spot-size is reduced from 30 μm to 5 μm . This is quite remarkable considering that the acoustic spot-size is 205 μm .

The simulation results were validated experimentally by flowing 3 μm diameter red-dyed polystyrene microspheres (Sigma Aldrich 42922) through a 200 μm inner diameter low-density polyethylene tube. The experimental configuration was similar to that shown in Fig. 1(a). The tube was illuminated with a pulsed laser at a wavelength of 532 nm, a pulse width of 0.5 ns, and a repetition rate of 1.0 kHz. The flow rate was controlled using a syringe pump and was high enough to ensure that there was no correlation between the photoacoustic signals observed in adjacent shots. The illumination spot-size was controlled with a variable beam expander and lens, and the optical fluence was kept below 20 mJ/cm^2 for all measurements. Photoacoustic signals were detected with a spherically focused 20 MHz transducer (Olympus V317). The receive-only beam width of the ultrasound transducer was determined by scanning the transducer over a 35 μm fiber and measuring the photoacoustic response. After deconvolution to take into account the finite size of the fiber, the receive beam width was found to be 208 μm . For each illumination spot-size, 5000 single-shot measurements were acquired using a high-speed digitizer and digitally processed with a 35 MHz low-pass second-order Butterworth filter.

Figure 2(a) shows the measured mean photoacoustic response, normalized by the pulse energy, for optical spot-sizes ranging from 8.8 to 39.6 μm and a particle concentration of $\rho = 0.3 \times 10^9$ particles/mL. In agreement with the simulation, very little change in the amplitude is seen over this spot-size range. Neglecting shot-to-shot intensity fluctuations in the laser, the measured standard deviation (σ_m) is the incoherent sum of both the system noise (σ_s) and that associated with the particle distribution (σ_p). σ_s is found by analyzing the data prior to the acoustic arrival, and the normalized standard deviation is then found through $\sigma_N = \sigma_p/A_{pp} = \sqrt{\sigma_m^2 - \sigma_s^2}/A_{pp}$ where σ_m is taken as the average value over a small time window centered over first positive peak. The results for two different particle concentrations are shown in Fig. 2(b). In contrast to the mean response, σ_N shows a marked increase as the spot diameter is decreased, an effect that is prominent even when the optical spot-size is more than an order or magnitude below the transducer spot-size. As expected, σ_N is higher for the lower particle concentration.

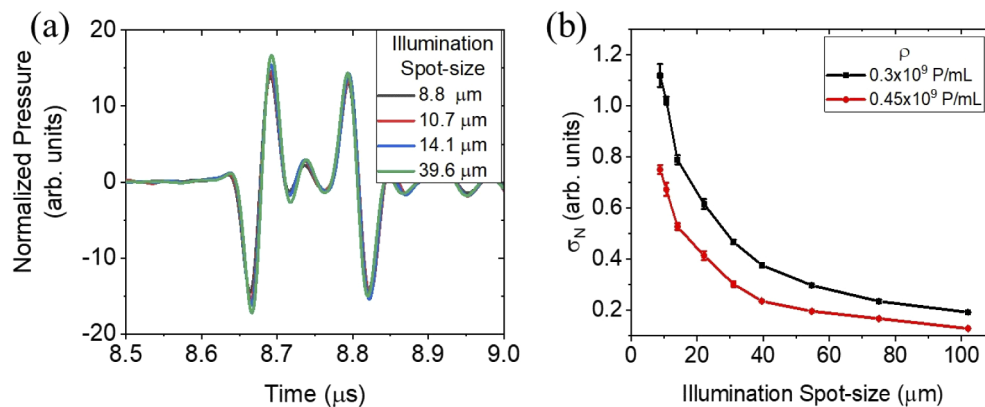


Fig. 2. Experimental investigation of the effect of spot-size on amplitude and variance of the photoacoustic response: (a) Mean photoacoustic signals, normalized by the incident energy, detected for a particle concentration of $\rho = 0.3 \times 10^9$ particles/mL for four illumination spot-sizes and (b) σ_N as a function of illumination spot-size for particle concentrations of $\rho = 0.3 \times 10^9$ particles/mL and $\rho = 0.45 \times 10^9$ particles/mL.

3. Results and discussion

We now turn our attention to using this physical effect as a guide star to focus light through a diffuse wall using optical wavefront shaping.

3.1. Experimental set-up for wavefront shaping

A schematic of the experimental setup is shown in Fig. 3. The active area of a liquid-crystal-on-silicon phase-only spatial light modulator (SLM) (512×512 pixels, Meadowlark P512-532) is illuminated with 7 ns pulses ($\lambda = 532$ nm, 20 kHz repetition rate) from a Q-switched diode-pumped solid-state laser (Mosaic 532-11). The incident power on the SLM is controlled using a variable attenuator, and a beam sampler is used to direct a small amount of light to a photodiode to trigger data acquisition. The SLM surface is imaged onto the back aperture of a $f = 75$ mm focal length lens and passed through an engineered diffuser (RPC Photonics EDC-1) to illuminate the sample with a speckle pattern. The sample is placed at the focal point of the lens and there is no measurable ballistic component of the optical field after the diffuser. The optical fluence at the sample plane is 2.44 mJ/cm². The speckle pattern at the focal plane is imaged using a CCD camera, and the ultrasound transducer and sample are the same as those described earlier.

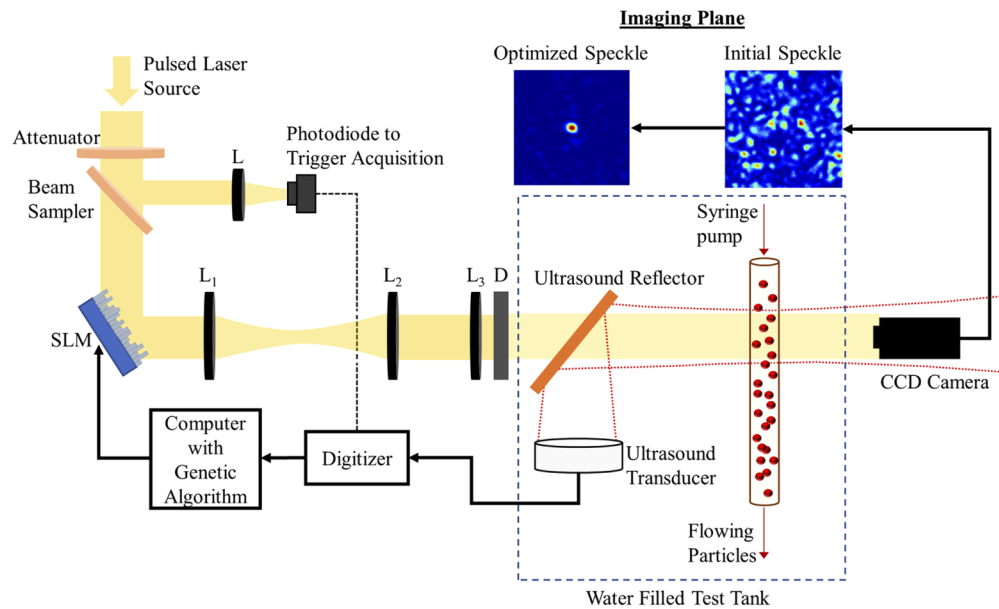


Fig. 3. A schematic of the experimental setup. The excitation pulse is reflected from the SLM and passed through a diffuser to create a speckle pattern at the target plane. Light is absorbed by the flowing particles and the resulting photoacoustic signal is detected by a focused ultrasound transducer. The CCD camera is used to image the speckle field before and after genetic algorithm optimization.

Photoacoustic guided wavefront optimization is performed using the genetic algorithm [8] and feeding back on either A_{pp} or the measured standard deviation σ_m . Note that again, the standard deviation of the amplitude at each time point is tracked, and σ_m is taken as the average value over a time window centered over the first arrival. For both feedback parameters, 5000 waveforms were collected to evaluate each phase pattern. At the conclusion of each optimization, the sample was translated out of the field of view of the CCD camera in order to acquire an image of the speckle field. The speckle size was taken as the FWHM of a Gaussian fit of the autocorrelation function along one of the axes.

3.2. Photoacoustic guided focusing through scattering media

A representative result for a particle concentration of $\rho = 0.3 \times 10^9$ particles/mL is given in Fig. 4. The initial speckle field prior to optimization is shown in Fig. 4(a), with a speckle size of $15.5 \mu\text{m}$. Figures 4(b) and 4(c) show the speckle field subsequent to wavefront optimization using A_{pp} and σ_m feedback signals, respectively. In both optimizations, the SLM pixels are binned into 32×32 even, independently controlled blocks and the optimization routine was terminated after 5000 iteration steps. The images are normalized by the average image intensity of the speckle field prior to optimization. Using A_{pp} feedback [Fig. 4(b)], the optical field is enhanced within the ultrasound focus but the field is distributed, and we were unable to focus the light to a single speckle. Defining the optical enhancement as the ratio of the peak intensity in the wavefront optimized image to the mean intensity of the initial speckle field, we observe an optical enhancement of 26. Five repetitions using A_{pp} feedback gave an average optical enhancement of 25 and the optical fields subsequent to optimization were similar to that shown in Fig. 4(b).

Wavefront shaping using σ_m feedback showed a significant improvement, leading to a highly localized optical field with a spot-size of approximately $17 \mu\text{m}$ (~ 12 times smaller than the

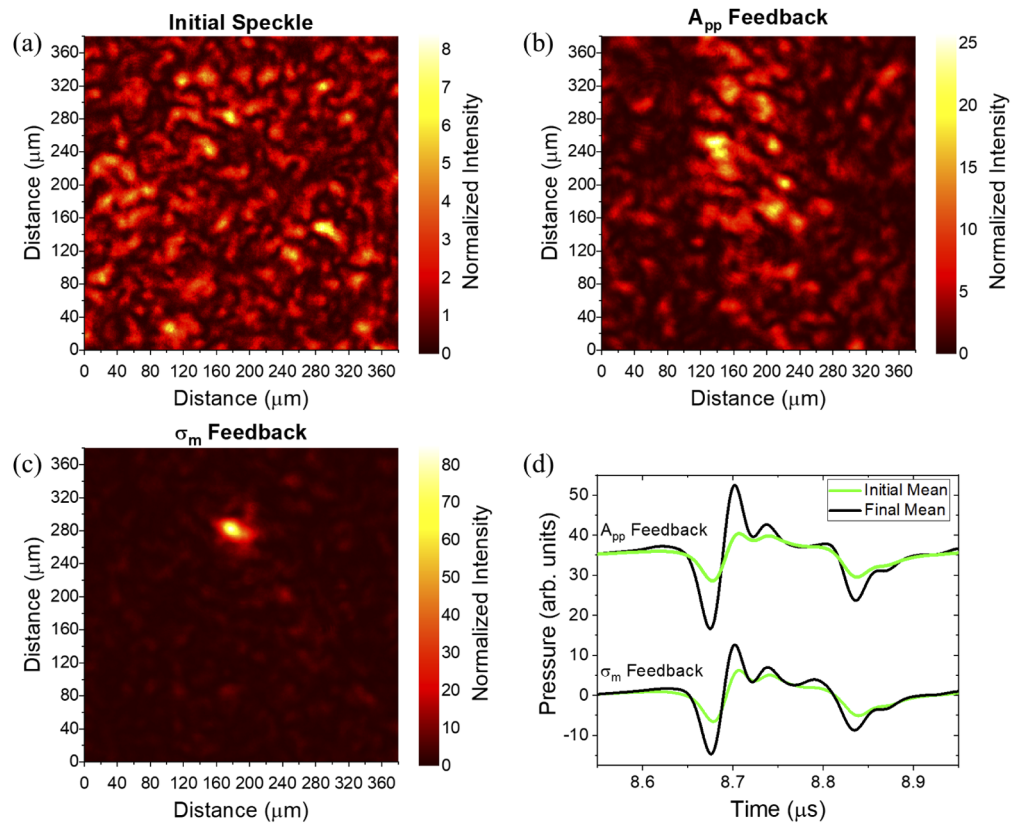


Fig. 4. Wavefront optimization results showing representative images of the speckle field (a) prior to wavefront optimization, (b) subsequent to wavefront optimization using A_{pp} as the feedback parameter, and (c) subsequent to wavefront optimization using σ_m as the feedback parameter. (d) Photoacoustic mean signals produced by the initial random speckle patterns (green curves) and the final speckle patterns using A_{pp} and σ_m feedback (black curves).

acoustic spot-size). The optical enhancement is 86 [Fig. 4(c)]. We again repeated the experiment five times and found that in all cases the light was concentrated in a region comparable to the speckle size, and the mean optical enhancement was 81. The standard deviation of the location of the focus in the five iterations was 20 μm , close to the speckle size. The measured enhancement is about an order or magnitude below the theoretical maximum [5]. We attribute this to the limited number of iterations, mechanical instability of the system throughout the optimization process, and measurement noise. Figure 4(d) shows the mean photoacoustic responses measured before and after optimization using A_{pp} and σ_m feedback, respectively. Remarkably, there is very little difference in the post-optimization photoacoustic signals.

One can better understand the advantage of optimizing using σ_m feedback by observing the evolution of the mean and standard deviation as the genetic algorithm progresses through phase patterns. Figure 5(a) shows how σ_m increases during optimizations using each type of feedback, while Fig. 5(b) shows the evolution of A_{pp} . Regardless of the feedback parameter used, both σ_m and A_{pp} increase during optimization. This is because σ_m increases linearly with A_{pp} and thus both parameters favor a large photoacoustic response.

The evolution of the normalized standard deviation σ_N is shown in Fig. 5(c). Note that σ_N is not a function of A_{pp} and any increase in σ_N during optimization can be attributed to a redistribution of light in the transducer focal zone rather than an increase in the integrated intensity.

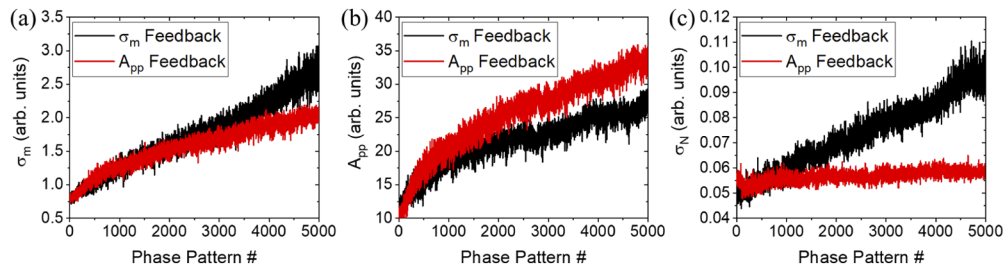


Fig. 5. The evolution of σ_m (a), A_{pp} (b) and σ_N (c) as the optimization routine iterates through 5000 phase patterns. On each plot, representative results found when using σ_m and A_{pp} as feedback parameters for the genetic algorithm are shown.

Indeed, when A_{pp} is used for feedback σ_N is relatively constant throughout the optimization. However, when σ_m is used as the feedback parameter, σ_N increases throughout the optimization as the light is focused to a single speckle.

This guide star mechanism relies on our ability detect the component of σ_m associated with the random distribution of particles (σ_p) in the presence of noise in the system including thermal noise in the transducer and detection electronics, as well as intensity fluctuations in

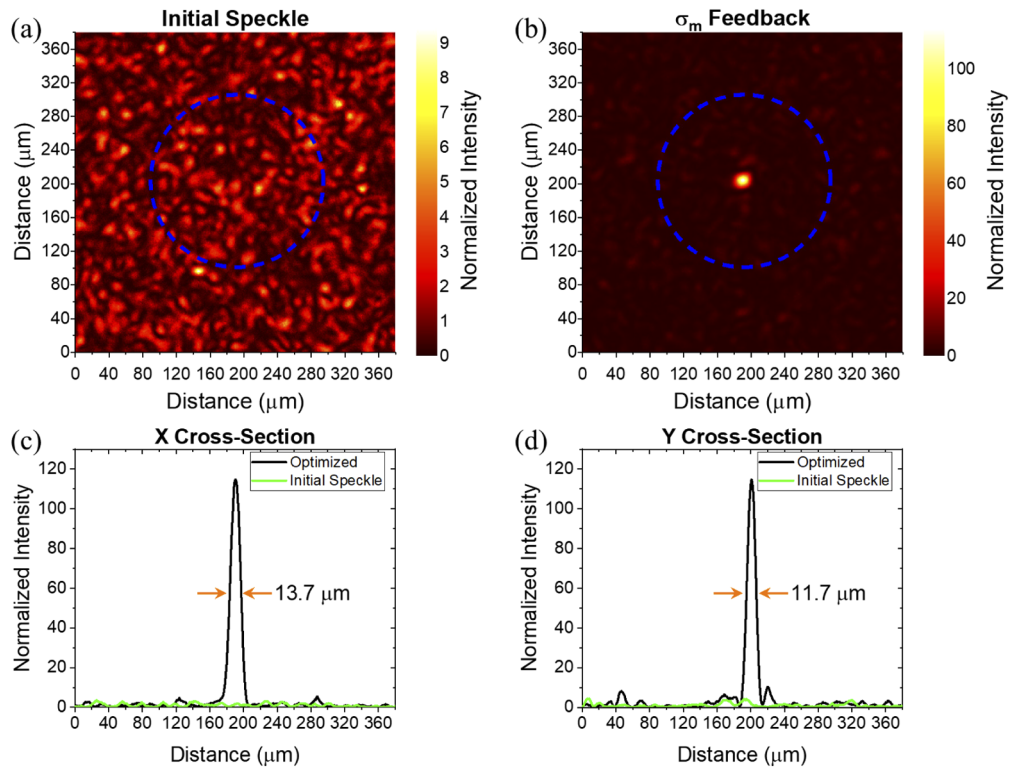


Fig. 6. Wavefront optimization results showing representative images of the speckle field (a) prior to wavefront optimization and (b) subsequent to wavefront optimization using σ_m as the feedback parameter. The dashed blue lines indicate the size of the acoustic focus (208 μm) and the speckle size is 10.3 μm . (c) Horizontal and (d) vertical cross-sections of the initial and optimized speckle field with the FWHM of the focused spot indicated.

the laser. At high particle concentrations, σ_p is very small with respect to A_{pp} while at very low particle concentrations σ_p is large with respect to A_{pp} but still a small value. Both of these limiting cases may make it difficult to distinguish σ_p from background noise sources and require additional measurements. Nevertheless, we find that the focusing approach is effective using other particle concentrations. Experiments performed using half the concentration ($\rho = 0.15 \times 10^9$ particles/mL), for example, gave similar results. Optimizations using σ_m feedback again led to localization of the light to a single speckle while those using A_{pp} had distributed illumination throughout the focal zone. The optical enhancement using σ_m and A_{pp} feedback were 101 and 25, respectively.

In the final experiment, the speckle size was reduced to $10.3 \mu\text{m}$ and the SLM was divided into 64×64 bins to access additional input modes. The particle concentration was $\rho = 0.3 \times 10^9$ particles/mL and the genetic algorithm was terminated after 8,000 SLM phase pattern iterations. The speckle pattern before optimization is shown in Fig. 6(a), while that after optimization using σ_m feedback is shown in Fig. 6(b). The field comes to a sharp focus after optimization. Horizontal and vertical lines across the focal point are shown in Fig. 6(c) and Fig. 6(d), respectively. The average FWHM of the focal spot from these two scans is $12.7 \mu\text{m}$, more than 16 times smaller than the size of the acoustic spot used to guide the focus. The resulting optical enhancement of the speckle field is 115.

4. Conclusion

In conclusion, we demonstrate a new nonlinear photoacoustic feedback mechanism for wavefront shaping that is based on the photoacoustic response from random distributions of flowing particles in a micro-vessel. The variation in this response over different random particle distributions increases dramatically as the light is localized. We use a genetic algorithm for optimization, and demonstrate that focusing through a diffuser is significantly more effective using the standard deviation of the photoacoustic signal as a feedback parameter than when using the mean. We demonstrate focusing of the optical field to a spot-size significantly smaller than the focal diameter of the transducer used to guide the focus. This sub-acoustic spot-size optical focus is achieved without a material nonlinearity and does not require high optical fluence. This technique may ultimately enable focusing on subsurface blood vessels for therapeutic applications or local imaging using, for example, the memory effect [35,36].

Funding

National Science Foundation (1548924, 1611513, 1810314); University of Colorado Boulder Imaging Science Interdisciplinary Research Theme; Max Kade Foundation.

Disclosures

The authors declare no conflicts of interest.

References

1. C. K. Kim, A. Adhikari, and K. Deisseroth, "Integration of optogenetics with complementary methodologies in systems neuroscience," *Nat. Rev. Neurosci.* **18**(4), 222–235 (2017).
2. T. J. Dougherty, C. J. Gomer, B. W. Henderson, G. Jori, D. Kessel, M. Korbek, J. Moan, and Q. Peng, "Photodynamic therapy," *J. Natl. Cancer Inst.* **90**(12), 889–905 (1998).
3. R. Weissleder and M. Nahrendorf, "Advancing biomedical imaging," *Proc. Natl. Acad. Sci. U. S. A.* **112**(47), 14424–14428 (2015).
4. V. Ntziachristos, "Going deeper than microscopy: the optical imaging frontier in biology," *Nat. Methods* **7**(8), 603–614 (2010).
5. I. M. Vellekoop and A. P. Mosk, "Focusing coherent light through opaque strongly scattering media," *Opt. Lett.* **32**(16), 2309–2311 (2007).
6. A. P. Mosk, A. Lagendijk, G. Leroose, and M. Fink, "Controlling waves in space and time for imaging and focusing in complex media," *Nat. Photonics* **6**(5), 283–292 (2012).

7. Z. Yaqoob, D. Psaltis, M. S. Feld, and C. Yang, "Optical phase conjugation for turbidity suppression in biological samples," *Nat. Photonics* **2**(2), 110–115 (2008).
8. D. B. Conkey, A. N. Brown, A. M. Caravaca-Aguirre, and R. Piestun, "Genetic algorithm optimization for focusing through turbid media in noisy environments," *Opt. Express* **20**(5), 4840–4849 (2012).
9. S. M. Popoff, G. Lerosey, R. Carminati, M. Fink, A. C. Boccara, and S. Gigan, "Measuring the transmission matrix in optics: an approach to the study and control of light propagation in disordered media," *Phys. Rev. Lett.* **104**(10), 100601 (2010).
10. C. L. Hsieh, Y. Pu, R. Grange, and D. Psaltis, "Digital phase conjugation of second harmonic radiation emitted by nanoparticles in turbid media," *Opt. Express* **18**(12), 12283–12290 (2010).
11. I. M. Vellekoop, E. G. van Putten, A. Lagendijk, and A. P. Mosk, "Demixing light paths inside disordered metamaterials," *Opt. Express* **16**(1), 67–80 (2008).
12. I. M. Vellekoop and C. M. Aegerter, "Scattered light fluorescence microscopy: imaging through turbid layers," *Opt. Lett.* **35**(8), 1245–1247 (2010).
13. E. G. van Putten, A. Lagendijk, and A. P. Mosk, "Optimal concentration of light in turbid materials," *J. Opt. Soc. Am. B* **28**(5), 1200–1203 (2011).
14. A. Boniface, B. Blochet, J. Dong, and S. Gigan, "Noninvasive light focusing in scattering media using speckle variance optimization," *Optica* **6**(11), 1381–1385 (2019).
15. H. Ruan, T. Haber, Y. Liu, J. Brake, J. Kim, J. M. Berlin, and C. Yang, "Focusing light inside scattering media with magnetic-particle-guided wavefront shaping," *Optica* **4**(11), 1337–1343 (2017).
16. H. Ruan, M. Jang, and C. Yang, "Optical focusing inside scattering media with time-reversed ultrasound microbubble encoded light," *Nat. Commun.* **6**(1), 8968 (2015).
17. E. H. Zhou, H. Ruan, C. Yang, and B. Judkewitz, "Focusing on moving targets through scattering samples," *Optica* **1**(4), 227–232 (2014).
18. C. Ma, X. Xu, Y. Liu, and L. V. Wang, "Time-reversed adapted-perturbation (TRAP) optical focusing onto dynamic objects inside scattering media," *Nat. Photonics* **8**(12), 931–936 (2014).
19. X. Xu, H. Liu, and L. V. Wang, "Time-reversed ultrasonically encoded optical focusing into scattering media," *Nat. Photonics* **5**(3), 154–157 (2011).
20. Y. M. Wang, B. Judkewitz, C. A. DiMarzio, and C. Yang, "Deep-tissue focal fluorescence imaging with digitally time-reversed ultrasound-encoded light," *Nat. Commun.* **3**(1), 928 (2012).
21. K. Si, R. Fiolka, and M. Cui, "Fluorescence imaging beyond the ballistic regime by ultrasound-pulse-guided digital phase conjugation," *Nat. Photonics* **6**(10), 657–661 (2012).
22. H. Ruan, M. Jang, B. Judkewitz, and C. Yang, "Iterative time-reversed ultrasonically encoded light focusing in backscattering mode," *Sci. Rep.* **4**(1), 7156 (2015).
23. J. W. Tay, P. Lai, Y. Suzuki, and L. V. Wang, "Ultrasonically encoded wavefront shaping for focusing into random media," *Sci. Rep.* **4**(1), 3918 (2015).
24. B. Judkewitz, Y. M. Wang, R. Horstmeyer, A. Mathy, and C. Yang, "Speckle-scale focusing in the diffusive regime with time reversal of variance-encoded light (TROVE)," *Nat. Photonics* **7**(4), 300–305 (2013).
25. F. Kong, R. H. Silverman, L. Liu, P. V. Chitnis, K. K. Lee, and Y. C. Chen, "Photoacoustic-guided convergence of light through optically diffuse media," *Opt. Lett.* **36**(11), 2053–2055 (2011).
26. A. M. Caravaca-Aguirre, D. B. Conkey, J. D. Dove, H. Ju, T. W. Murray, and R. Piestun, "High contrast three-dimensional photoacoustic imaging through scattering media by localized optical fluence enhancement," *Opt. Express* **21**(22), 26671–26676 (2013).
27. T. Chainge, O. Katz, A. C. Boccara, M. Fink, E. Bossy, and S. Gigan, "Controlling light in scattering media non-invasively using the photoacoustic transmission matrix," *Nat. Photonics* **8**(1), 58–64 (2014).
28. D. B. Conkey, A. M. Caravaca-Aguirre, J. D. Dove, H. Ju, T. W. Murray, and R. Piestun, "Super-resolution photoacoustic imaging through a scattering wall," *Nat. Commun.* **6**(1), 7902 (2015).
29. P. Lai, L. Wang, J. W. Tay, and L. V. Wang, "Photoacoustically guided wavefront shaping for enhanced optical focusing in scattering media," *Nat. Photonics* **9**(2), 126–132 (2015).
30. Z. Guo, L. Li, and L. V. Wang, "On the speckle-free nature of photoacoustic tomography," *Med. Phys.* **36**(9Part1), 4084–4088 (2009).
31. Z. Guo, Z. Xu, and L. V. Wang, "Dependence of photoacoustic speckles on boundary roughness," *J. Biomed. Opt.* **17**(4), 046009 (2012).
32. X. L. Deán-Ben and D. Razansky, "On the link between the speckle free nature of optoacoustics and visibility of structures in limited-view tomography," *J. Photoacoust.* **4**(4), 133–140 (2016).
33. J. Gateau, T. Chaigne, O. Katz, S. Gigan, and E. Bossy, "Improving visibility in photoacoustic imaging using dynamic speckle illumination," *Opt. Lett.* **38**(23), 5188–5191 (2013).
34. L. Li and L. V. Wang, "Speckle in photoacoustic tomography," *Proc. SPIE* **6086**, 60860Y (2006).
35. I. Freund, M. Rosenbluh, and S. Feng, "Memory effects in propagation of optical waves through disordered media," *Phys. Rev. Lett.* **61**(20), 2328–2331 (1988).
36. S. Feng, C. Kane, P. A. Lee, and A. D. Stone, "Correlations and fluctuations of coherent wave transmission through disordered media," *Phys. Rev. Lett.* **61**(7), 834–837 (1988).